Rapid Communications

Vibrational relaxation dynamics of the nitrogen-vacancy center in diamond

Ronald Ulbricht,[1,2,*] Shuo Dong,[2] Adam Gali,[3,4] Sheng Meng,[5,6] and Zhi-Heng Loh[1,2,7,†]

[1]*Division of Chemistry and Biological Chemistry, School of Physical and Mathematical Sciences, Nanyang Technological University, Singapore 637371, Singapore*

[2]*Division of Physics and Applied Physics, School of Physical and Mathematical Sciences, Nanyang Technological University, Singapore 637371, Singapore*

[3]*Wigner Research Centre for Physics, Hungarian Academy of Sciences, P.O. Box 49, H-1525 Budapest, Hungary*

[4]*Department of Atomic Physics, Budapest University of Technology and Economics, Budafoki út 8., H-1111 Budapest, Hungary*

[5]*Beijing National Laboratory for Condensed Matter Physics and Institute of Physics, Chinese Academy of Sciences, Beijing 100190, People's Republic of China*

[6]*Collaborative Innovation Center of Quantum Matter, Beijing 100190, People's Republic of China*

[7]*Centre for Optical Fibre Technology, The Photonics Institute, Nanyang Technological University, 50 Nanyang Avenue, Singapore 639798, Singapore*

(Received 13 April 2018; revised manuscript received 21 May 2018; published 8 June 2018)

We employ a combination of spectrally resolved optical pump-probe spectroscopy and excited-state *ab initio* molecular dynamics (ESAIMD) simulations to study the ultrafast vibrational relaxation dynamics of the ^3E excited state of negatively charged nitrogen vacancy (NV^-) defects. The experimental results reveal vibrational relaxation in the phonon sideband with a time constant of approximately 50 fs, in excellent agreement with the ~40-fs structural equilibration timescale predicted by ESAIMD simulations. The observed ultrafast vibrational energy relaxation implies that dynamical processes triggered by photoexcitation into the phonon sideband of the NV^- center occur primarily in the lowest vibronic level of the ^3E state.

DOI: 10.1103/PhysRevB.97.220302

The identification of deep-level defects in semiconductors—also known as color centers—with unique properties has inspired new research directions to utilize them in novel quantum technologies [1]. Diamond has emerged as a popular host medium, in particular, due to its remarkable material properties and relative ease of fabrication [2]. Among its known color centers, the negatively charged nitrogen-vacancy (NV^-) defect, consisting of a nitrogen atom (N) substituting a carbon atom (C) adjacent to a missing carbon atom, i.e., vacancy (V), in the diamond lattice [see the inset in Fig. 1(a)], is particularly attractive due to its highly localized and isolated electronic states. Advances in the magnetic and optical manipulation of their quantum states herald their application to spintronics [3] and photonics [4]. In addition, nanoscale magnetic and temperature sensors, as well as highly luminescent, photostable biomarkers and single-photon sources based on single NV^- defects have also been demonstrated [5,6].

The electronic structure of the NV^- defect is dictated by its six constituent electrons, which derive from the lone pair of the nitrogen atom, the dangling bonds of the three carbon atoms surrounding the vacancy, and the excess negative charge trapped at the defect which is donated by other defects in diamond. Occupation of these localized molecular orbitals furnishes a $^3A_2$ electronic ground state, whose optical transition to the ^3E excited state is characterized by a narrow zero-phonon line (0PL) at 637 nm. This excitation can be well described by promoting an electron from the a_1 highest occupied molecular orbital (HOMO) to the double degenerate e lowest unoccupied molecular orbital (LUMO) in the spin minority channel where the levels of these orbitals occur in the wide band gap of diamond [7,8]. In addition to the 0PL, vibronic coupling gives rise to a broad phonon sideband in which peaks are spaced apart by ~67 meV [9], creating one-phonon line (1PL) and two-phonon line (2PL) peaks. These peaks are particularly distinct at cryogenic temperatures, appearing to the blue (red) side of the 0PL in absorption (photoluminescence) [see Fig. 1(a)]. This vibronic progression arises from the interaction of the ^3E electronic state with totally symmetric, quasilocalized vibrational modes (qLVMs) that involve the displacement of the nitrogen atom and the carbon atoms surrounding the vacancy [10].

The utility of the NV^- defect for harnessing coherent spin dynamics in the electronic ground state relies on the reproducible initialization of the spin state through optical pumping. This is often achieved by off-resonant excitation, i.e., above the 0PL transition into the phonon sideband. In those cases the spin polarization is commonly limited to about 90% [11]. Conversely, resonant excitation at the 0PL has been shown to reach almost unity spin polarization [12]. It is thus surprising that, even though numerous studies of the NV^- defect rely on the photoexcitation of its phonon sideband [11,13], the vibrational relaxation dynamics of the ^3E excited state remains largely unexplored. Recently, an investigation by femtosecond transient grating spectroscopy yielded a timescale of ~4 ps for vibrational relaxation within the phonon sideband [14]. In that

*ronald.ulbricht@colorado.edu
†zhiheng@ntu.edu.sg

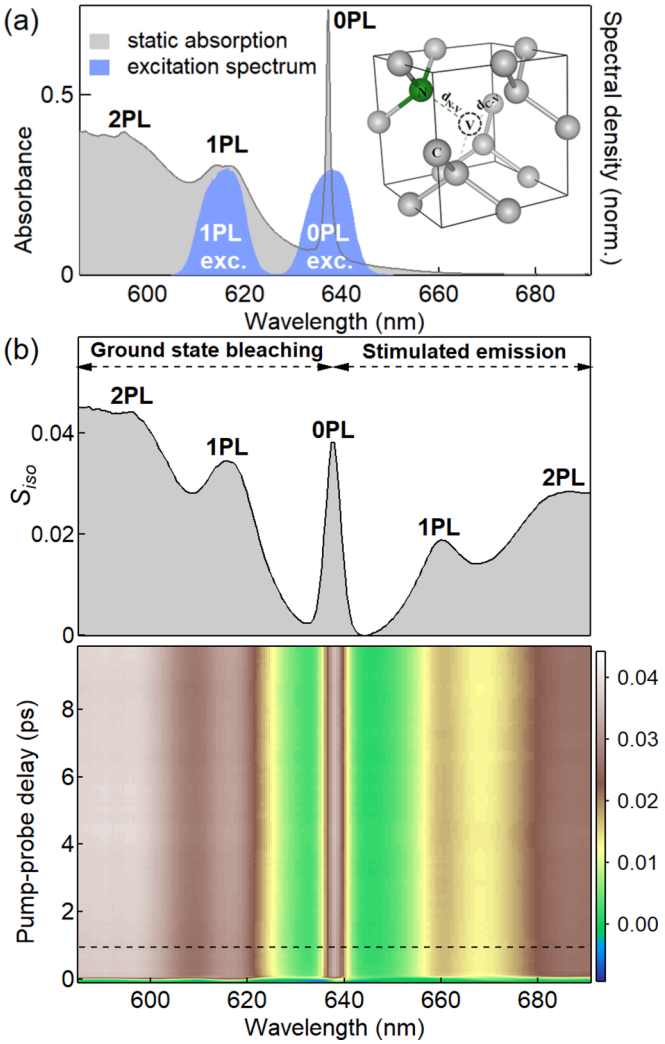

FIG. 1. (a) Optical absorption spectrum of the NV^- sample recorded at 77 K, revealing clear zero-phonon line (0PL), one-phonon line (1PL), and two-phonon line (2PL) transitions. The spectra of the pump pulses used to excite the 0PL and 1PL transitions are also shown as blue shaded; the inset illustrates the structure of the NV^- defect within the diamond lattice, indicating the distances between vacancy and nitrogen atoms $d_{N\text{-}V}$ (green dashed line), as well as between vacancy and carbon atoms $d_{C\text{-}V}$ (gray dashed line); (b) Time-resolved, isotropic differential transmission spectra S_{iso} after 1PL photoexcitation (lower panel). The upper panel shows the S_{iso} spectrum obtained at a time delay of 1 ps (dashed black line in the lower panel), depicting ground-state bleaching on the blue side of the 0PL and stimulated emission on the red side of the 0PL.

study, the use of broadband laser pulses with a spectral bandwidth that encompassed the 0PL and the two lowest-energy satellites (1PL and 2PL) in the phonon sideband allowed the elucidation of multiple vibrational modes which couple to the $^3A_2 \rightarrow {}^3E$ optical transition.

Here, we employ femtosecond optical pump-probe spectroscopy to resolve the ultrafast vibrational relaxation dynamics of the NV^- ^3E state following selective excitation of the one-phonon (1PL) satellite in the phonon sideband [Fig. 1(a)]. Vibrational relaxation with a time constant of less than 50 fs is observed, i.e., two orders of magnitude faster than previously reported [14]. Excited-state *ab initio* molecular dynamics (ESAIMD) simulations of an NV^- center embedded in a diamond quantum dot reveal equilibration of the structure within ~40 fs following HOMO-LUMO photoexcitation, in excellent agreement with the experimental results.

The experiments are performed on an ensemble of NV^- defects by using a narrow-band pump of 10-nm bandwidth to selectively excite either the 1PL or the 0PL transitions [Fig. 1(a)], and a ~10-fs broadband probe that covers the spectral range of 580–700 nm [Fig. 1(b)]. The instrument response as measured by cross correlation is 80 fs [full width at half maximum (FWHM)], limited by the duration of the pump pulse, which is ~1.3× its transform-limited duration [11,15–27]. The ultrafast excited-state dynamics of the NV^- defect is reconstructed from two sets of normalized differential transmission measurements—one in which the pump and probe beams have parallel polarizations, and another one in which the polarizations are perpendicular [15]. The normalized differential transmission signal is defined as $S^i(\lambda,t) = [T^i_{on}(\lambda,t) - T^i_{off}(\lambda,t)]/T^i_{off}(\lambda,t)$, where i denotes the polarization index ($\parallel$ or $\perp$), λ is the probe wavelength, t is the pump-probe time delay, and T_{on} (T_{off}) is the sample transmission in the presence (absence) of the photoexcitation pump pulse [Fig. 1(c)]. The signals recorded with different relative polarizations between the pump and probe pulses can be further combined to yield the isotropic signal, given as $S_{iso} = (S^{\parallel} + 2S^{\perp})/3$. S_{iso} reflects the population dynamics of vibronic levels, independent of electronic reorientation dynamics that accompanies orbital dephasing [28–30]. Comparing the femtosecond population dynamics between excitation to the vibrational ground state (0PL excitation) and to a vibrationally excited state (1PL excitation) of the ^3E state reveals the vibrational relaxation time.

The time evolution of the differential transmission spectra $S_{iso}(\lambda,t)$ collected after 1PL excitation of the NV^- sample at 77 K is shown in Fig. 1(b), together with a spectral line-out at a time delay of 1 ps. The narrow, positive differential transmission feature at 637 nm is due to ground-state bleaching (GSB) of the 0PL transition and stimulated emission (SE) from the ^3E excited state. Additional positive differential transmission observed to the blue (red) sides of the 0PL can be attributed to GSB (SE), which resembles steady-state absorption (PL) spectra [Fig. 1(a)]). Although excited-state absorption of the ^3E state to the conduction band occurs within the probe spectral range as well, its contribution to the differential transmission signal is expected to be minor due to the low oscillator strengths associated with continuum transitions. The presence of single-substitutional nitrogen defects N_s, which have a low ionization potential of ~1.7 eV, suggests that photoexcitation of the NV^- 0PL can also trigger the injection of N_s electrons into the conduction band. Control experiments that employ 670-nm excitation, i.e., below the 0PL, show that ionization of the N_s defect leads to a <5% decrease of S_{iso} at photoexcitation and a subsequent few-picosecond recovery over the entire probe spectral range, which presumably arises from the recapture of the conduction band electrons in the N_s defects [15]. Such picosecond recombination dynamics after excitation of N_s defects have been reported before [26].

Apart from this contribution, S_{iso} from 1PL excitation does not, at first glance, appear to exhibit any dynamics that can

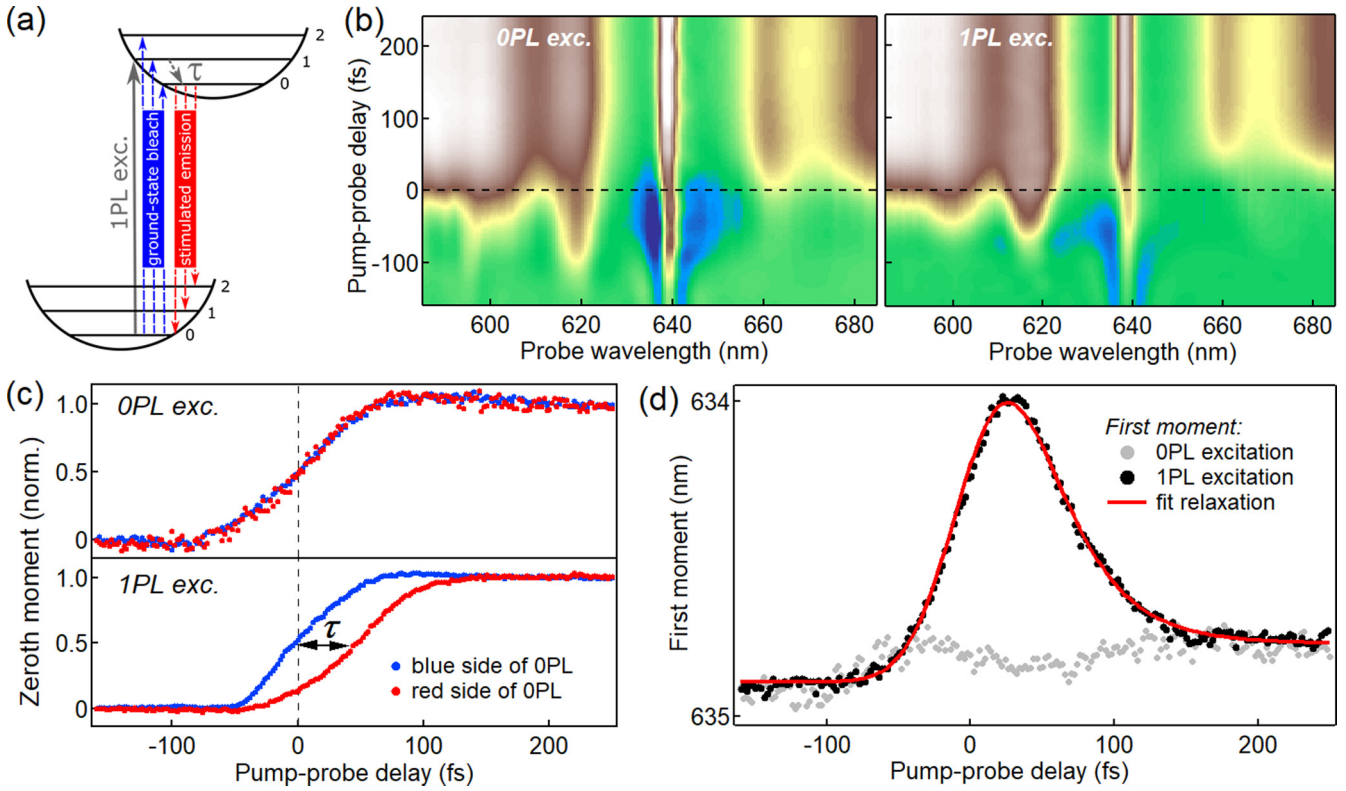

FIG. 2. (a) Schematic of monitoring the vibrational relaxation process: 1PL excitation (gray solid arrow) creates population at $v' = 1$ in the excited state (accompanied by GSB of the probe to the blue side of the 0PL, blue arrows) that subsequently relaxes to the vibrational ground state $v' = 0$ within the time τ (gray dashed arrow). Stimulated emission on the red side of the 0PL probe spectrum (red arrows) occurs when population has relaxed. (b) Early-time S_{iso} spectra obtained after 0PL excitation (left) and 1PL excitation (right). (c) Zeroth moment of S_{iso} for 0PL excitation (upper panel) and 1PL excitation (lower panel) of the probe on the blue side and red side of the 0PL; the time shift between the zeroth momenta of blue and red sides of 1PL excitation give the relaxation time τ. (d) First moment of S_{iso} for 0PL excitation (gray dots) and 1PL excitation (black dots). The black line is a fit of the 1PL data to the relaxation model.

be assigned to the NV^- center within our 20-ps measurement time window, rendering the 1PL excitation results practically identical to the 0PL excitation. In particular, we do not observe any signatures of the ~4-ps vibrational relaxation as reported in Ref. [14]. "Hot" vibronic states, as created after 1PL excitation, ought to exhibit a change in S_{iso} due to the different Franck-Condon (FC) factors associated with their transitions to the electronic ground state [see Fig. 2(a) and Ref. [15]]. Such long relaxation dynamics should be clearly visible in our measurements as a decay or rise of S_{iso} in certain spectral probe regions over the alleged relaxation timescale of 4 ps. This is, however, not observed.

Close examination of the 0PL- and 1PL-excited data sets reveal subtle differences within the first 100 fs after photoexcitation. Figure 2(b) shows the time-resolved differential transmission spectra obtained with both excitation scenarios for the first 250 fs. The noticeable difference between both data sets is the ~50-fs delayed onset of SE on the red side of the zero-phonon line (0PL) for 1PL excitation as compared to 0PL excitation. In order to evaluate the dynamics and extract a vibrational relaxation time τ, we calculate both the zeroth moment, defined as $M_0(\lambda,t) = \int_{\lambda_1}^{\lambda_2} S_{iso}(\lambda,t)d\lambda$, and the first moment, $M_1(\lambda,t) = \int_{\lambda_1}^{\lambda_2} \lambda\ S_{iso}(\lambda,t)d\lambda / \int_{\lambda_1}^{\lambda_2} S_{iso}(\lambda,t)d\lambda$ of the transient spectra.

The zeroth moment $M_0(\lambda,t)$ was computed for both excitation scenarios on the red side of the 0PL probe transition over the spectral range from 660 to 690 nm, and on the blue side from 580 to 610 nm. The blue side is predominantly sampling the GSB, which is established at the time of photoexcitation, i.e., at time zero, whereas the red side probes SE, which in turn has reached its equilibrium spectral shape resembling PL when $v' = 0$ is populated after the vibrational relaxation time τ. The results are shown in Fig. 2(c). Since 0PL excitation directly populates the vibrational ground state [Fig. 2(c) upper panel], both GSB (blue) and SE (red) are established congruently at time zero. The situation is different for 1PL excitation [Fig. 2(c) lower panel]: Here, the onset of SE (red) is clearly delayed with respect to GSB (blue) by the vibrational relaxation time τ. A set of seven independent measurements for 1PL excitation gives $\tau = 45 \pm 10$ fs.

We use the first moment $M_1(\lambda,t)$, which calculates the spectral weight of the differential probe spectrum, as a second measure for obtaining τ. For this, we evaluate $M_1(\lambda,t)$ over the spectral range of 580–700 nm. We exclude the regions around the 0PL and 1PL excitation pulses (610–650 nm) to avoid coherent artifacts that can give erroneous signal contributions around the region of pump-probe spectral and temporal overlap. The results are shown in Fig. 2(d). $M_1(\lambda,t)$

for 0PL excitation (gray solid circles) stays practically constant, indicating no changes in the spectral weight of the probe spectrum as a function of time delay. In stark contrast, for the 1PL excitation (black solid circles), $M_1(\lambda,t)$ shows a clear blue shift, followed by a redshift—a clear indication for changes in spectral weight due to the delayed onset of SE. To quantify the timescale, we fit $M_1(\lambda,t)$ from seven independent measurements to a convolution of the instrument response function with an exponential decay $M_1(t) = Ae^{-t/\tau} + a$, where A is the amplitude of the decay and a is an offset. An example fit is shown as the red graph in Fig. 2(d). The results yield $\tau = 30 \pm 7$ fs, which is slightly lower than the value of τ obtained from the zeroth moment results. Please note, however, that the values for both zero and first moments are below the instrument response of our measurement, thus ultimately only permitting an upper bound of $\tau \leqslant 50$ fs on the vibrational relaxation timescale.

Interestingly, the noticeable delay in the appearance of the S_{iso} signal between the red and blue regions observed with 1PL excitation, as is evident in $M_0(\lambda,t)$ in Fig. 2(c), suggests negligible SE from the $v' = 1$ vibrational level of the electronic excited state. Even though the vibrational relaxation is faster than the instrument response, which diminishes the signal from the vibrationally excited population, we would still expect to see a finite signal due to the significant FC factor of some SE transitions from $v' = 1$, particularly at the 0PL and 1PL (660-nm) probe wavelength [15]. We, however, do not observe any such transient signal or any other signatures of SE before the system has relaxed. This is somewhat surprising since PL and absorption spectra of NV^- are practically symmetric, indicating equal FC factors for GSB and SE. This behavior could possibly be related to the conical intersection between the two degenerate excited states, created as a result of the Jahn-Teller distortion [31,32], that gives rise to additional ultrafast dynamics that is neither captured by our measurements, nor by steady-state PL and absorption. In fact, sub-100-fs nonadiabatic dynamics has been reported before [30].

ESAIMD simulations of the NV^- defect based on time-dependent density functional theory reveal ultrafast structural reorganization immediately following HOMO-LUMO electronic excitation (Fig. 3) [15]. To this end, the time-dependent interatomic distances are calculated for the N-V and C-V distances. The position of the vacancy is defined by the translational symmetry of the diamond lattice where the lattice points can be derived from the carbon atoms that are far from the defect. Starting from an initial N-V distance of 1.71 Å in the ground state, the N-V distance decreases to 1.62 Å within ~40 fs of electronic excitation, thereafter oscillating in the range of 1.61−1.63 Å. On the other hand, the C-V distances increase from 1.64 to 1.74 Å within 30 fs before oscillating between 1.68 and 1.72 Å. Thus, the C-V and N-V equilibrium distances are interchanged in the ground state and excited state. This switch of N-V and C-V bond length upon photoexcitation originates from the character of electron orbitals involved: The a_1 state is strongly localized on the N atom and the three C atoms whereas the e state is only localized on the three C atoms. Thus, the N atom is strongly spin polarized in the ^3E state compared to $^3A_2$ state, while the C ligands will be somewhat less spin polarized, which

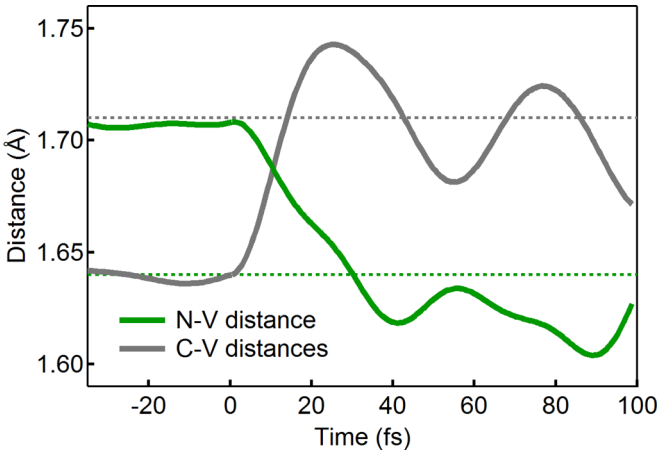

FIG. 3. Simulated ESAIMD trajectories for N-V (green line) and C-V distances (gray line). At $t = 0$ fs, an electron is promoted from the a_1 HOMO to the e LUMO, representative of the electronic excitation of the NV^- defect. The dashed lines indicate the calculated equilibrium distances of the ^3E excited state.

induces different charge transfers between the atoms in the ^3E state, and leads to the shortening of the N-V distance and elongation of the C-V distances [19]. In fact, the atomic geometry furnished after 40 fs is very similar to the optimized structure of the NV^- center in its electronic excited state [19], of which the equilibrium distances are shown as dashed lines in Fig. 3, providing evidence that the relaxed excited-state structure has been reached. The calculated timescale for structural equilibration in the electronic excited state of the NV^- defect is consistent with the <50-fs dynamics observed in the pump-probe experiment. These observations strongly support the assignment of the experimentally observed <50-fs dynamics to vibrational relaxation of the NV^- defect in its ^3E excited state.

It is interesting to note that the ~50-fs timescale determined for vibrational energy redistribution in the NV^- defect is much faster than what is usually observed. The qLVM that couples to the electronic transition has an energy of ~67 meV, which corresponds to a cycle period of 60 fs. The relaxation thus occurs within one vibrational period, which is exceptionally fast. We are currently unable to provide a conclusive explanation for this phenomenon, which would constitute an interesting subject for further studies, but would like to speculate on possible mechanisms. First, the ultrafast vibrational relaxation could be facilitated by the anharmonic coupling of the optically excited, totally symmetric (a_1) qLVM to the high phonon density of states that peaks at ~70 meV [33,34]. Some of these phonon modes, which have e symmetry, are not accessed by optical excitation. Resonant energy transfer from the optically excited a_1 mode to the phonon modes of e symmetry can support the ultrafast vibrational relaxation observed herein. The second possibility is to consider vibrational conical intersections, which have been invoked to explain ~100-fs vibrational relaxation times [35,36]. In vibrational conical intersections, two high-frequency modes q_1 and q_2 are coupled to the same two low-frequency modes Q_1 and Q_2 such that the two high-frequency modes become

energetically degenerate at a given (Q_1, Q_2) configuration. If one of these high-frequency modes corresponds to the a_1 qLVM, the presence of the vibrational conical intersection would facilitate its ultrafast relaxation to the other high-frequency mode.

Our vibrational relaxation time is almost two orders of magnitude shorter than the ∼4-ps exponential decay that was previously determined by femtosecond transient grating spectroscopy [14]. We are currently unable to provide a conclusive explanation for this discrepancy. A possible consideration could be the different excitation conditions of the two studies—the transient grating measurement was performed with broadband pulses that span the 0PL, 1PL, and 2PL transitions, whereas the present work employs the selective excitation of the 1PL satellite. In the case of broadband photoexcitation, the creation of a large, nonequilibrium population of low-frequency bath mode phonons, as evidenced by the multitude of low-frequency coherent phonons observed therein, can potentially suppress vibrational relaxation rates due to the hot phonon effect [37], resulting in a slower relaxation observed in the transient grating measurement. Future experiments that emulate the excitation conditions of Ref. [14] should allow one to resolve the discrepancy between the results obtained from the two studies.

In conclusion, femtosecond optical pump-probe spectroscopy has been used to elucidate the ultrafast vibrational relaxation dynamics in the excited state of the NV^- defect in diamond following the photoexcitation of its one-phonon satellite. The vibrational relaxation of the excited 67-meV qLVM is characterized by a decay constant of approximately 50 fs. Given its ultrashort timescale, vibrational energy redistribution is likely to precede over other fundamental processes that occur in the ^3E excited state of the NV^- defect, such as the two-phonon Raman-type population transfer between the components of the orbital doublets, characterized by a time constant of ∼5 ps at 77 K [13]. This implies that various photoinduced phenomena involving the NV^- ^3E state occur primarily in the $v' = 0$ vibrational ground state, even in the case of experimental schemes that employ excitation into the phonon sideband [11,13].

This work is supported by a startup grant from NTU, the A*Star SERC Public Sector Funding (122-PSF-0011), the Ministry of Education Academic Research Fund (MOE2014-T2-2-052 and RG105/17), and the award of a Nanyang Assistant Professorship to Z.-H.L. R.U. acknowledges support by a DFG fellowship (UL 474/1-1). S.M. acknowledges financial support from MOST (Grant No. 2016YFA0300902) and NSFC (Grant No. 11774396). A.G. acknowledges the National Research Development and Innovation Office of Hungary (NKFIH) within the Quantum Technology National Excellence Program (Project No. 2017-1.2.1-NKP-30-2017-00001) and QuantERA Q-Magine Project (Grant No. 127889). We are grateful to H.-D. Kim and D. M. Jonas for useful discussions, to R. U. A. Khan for experimental assistance, and to J. Schwartz for providing the sample.

[1] J. R. Weber, W. F. Koehl, J. B. Varley, A. Janotti, B. B. Buckley, C. G. Van de Walle, and D. D. Awschalom, Proc. Natl. Acad. Sci. U.S.A. **107**, 8513 (2010).
[2] I. Aharonovich, A. D. Greentree, and S. Prawer, Nat. Photonics **5**, 397 (2011).
[3] V. V. Dobrovitski, G. D. Fuchs, A. L. Falk, C. Santori, and D. D. Awschalom, Annu. Rev. Condens. Matter Phys. **4**, 23 (2013).
[4] R. Hanson and D. D. Awschalom, Nature (London) **453**, 1043 (2008).
[5] I. Aharonovich and E. Neu, Adv. Opt. Mater. **2**, 911 (2014).
[6] R. Schirhagl, K. Chang, M. Loretz, and C. L. Degen, Annu. Rev. Phys. Chem. **65**, 83 (2014).
[7] A. Gali, E. Janzen, P. Deak, G. Kresse, and E. Kaxiras, Phys. Rev. Lett. **103**, 186404 (2009).
[8] J. P. Goss, R. Jones, S. J. Breuer, P. R. Briddon, and S. Oberg, Phys. Rev. Lett. **77**, 3041 (1996).
[9] G. Davies, J. Phys. C **7**, 3797 (1974).
[10] A. Gali, T. Simon, and J. E. Lowther, New J. Phys. **13**, 025016 (2011).
[11] M. W. Doherty, N. B. Manson, P. Delaney, F. Jelezko, J. Wrachtrup, and L. C. L. Hollenberg, Phys. Rep. **528**, 1 (2013).
[12] L. Robledo, L. Childress, H. Bernien, B. Hensen, P. F. A. Alkemade, and R. Hanson, Nature (London) **477**, 574 (2011).
[13] K.-M. C. Fu, C. Santori, P. E. Barclay, L. J. Rogers, N. B. Manson, and R. G. Beausoleil, Phys. Rev. Lett. **103**, 256404 (2009).
[14] V. M. Huxter, T. A. A. Oliver, D. Budker, and G. R. Fleming, Nat. Phys. **9**, 744 (2013).
[15] See Supplemental Material at http://link.aps.org/supplemental/10.1103/PhysRevB.97.220302 for additional information on the experiments, data analysis, and simulations, which includes Refs. [16–27].
[16] A. L. Dobryakov, S. A. Kovalenko, and N. P. Ernsting, J. Chem. Phys. **119**, 988 (2003).
[17] A. Gali, Phys. Rev. B **79**, 235210 (2009).
[18] A. Gali, Phys. Status Solidi **248**, 1337 (2011).
[19] A. Gali, M. Fyta, and E. Kaxiras, Phys. Rev. B **77**, 155206 (2008).
[20] F. J. Heremans, G. D. Fuchs, C. F. Wang, R. Hanson, and D. D. Awschalom, Appl. Phys. Lett. **94**, 152102 (2009).
[21] K. Ishioka, M. Hase, M. Kitajima, and H. Petek, Appl. Phys. Lett. **89**, 231916 (2006).
[22] J. Jaumot, A. de Juan, and R. Tauler, Chemom. Intell. Lab. Syst. **140**, 1 (2015).
[23] S. Meng and E. Kaxiras, J. Chem. Phys. **129**, 054110 (2008).
[24] C. Ruckebusch, M. Sliwa, P. Pernot, A. de Juan, and R. Tauler, J. Photochem. Photobiol. C **13**, 1 (2012).
[25] J. M. Soler, E. Artacho, J. D. Gale, A. Garcia, J. Junquera, P. Ordejon, and D. Sanchez-Portal, J. Phys.: Condens. Matter **14**, 2745 (2002).
[26] R. Ulbricht, S. T. van der Post, J. P. Goss, P. R. Briddon, R. Jones, R. U. A. Khan, and M. Bonn, Phys. Rev. B **84**, 165202 (2011).
[27] J. Weber and G. Hohlneicher, Mol. Phys. **101**, 2125 (2003).
[28] D. A. Farrow, W. Qian, E. R. Smith, A. A. Ferro, and D. M. Jonas, J. Chem. Phys. **128**, 144510 (2008).
[29] K. Wynne and R. M. Hochstrasser, Chem. Phys. **171**, 179 (1993).

[30] R. Ulbricht, S. Dong, I. Y. Chang, B. M. K. Mariserla, K. M. Dani, K. Hyeon-Deuk, and Z. H. Loh, Nat. Commun. **7**, 13510 (2016).
[31] T. A. Abtew, Y. Y. Sun, B. C. Shih, P. Dev, S. B. Zhang, and P. Zhang, Phys. Rev. Lett. **107**, 146403 (2011).
[32] G. Thiering and A. Gali, Phys. Rev. B **96**, 081115 (2017).
[33] T. Elsaesser and W. Kaiser, Annu. Rev. Phys. Chem. **42**, 83 (1991).
[34] J. Zhang, C.-Z. Wang, Z. Z. Zhu, and V. V. Dobrovitski, Phys. Rev. B **84**, 035211 (2011).
[35] P. Hamm and G. Stock, Phys. Rev. Lett. **109**, 173201 (2012).
[36] B. P. Thapaliya, M. B. Dawadi, C. Ziegler, and D. S. Perry, Chem. Phys. **460**, 31 (2015).
[37] J. Shah, *Ultrafast Spectroscopy of Semiconductors and Semiconductor Nanostructures*, Springer Series in Solid-State Sciences (Springer, Berlin, 1999).